RSC Advances

PAPER

View Article Online
View Journal | View Issue

Cite this: *RSC Adv.*, 2025, **15**, 2591

Assessment of antimicrobial efficacy of leather coating using chitosan modified TiO_2–CuO nanocomposites†

Vijay S. Ghodake,[ab] Pramod A. Koyale,[c] Vikramsinh B. More,[d] Kailas D. Sonawane[ad] and Sagar D. Delekar*[a]

This research investigates the microbial inactivation potential of ternary TiO_2–CuO–chitosan nanocomposites (TCC NCs) applied as surface coatings on cowhide leather. Initially, bare TiO_2 nanoparticles (NPs) and binary TiO_2–CuO (TC) NCs, with varying CuO NPs content, were prepared using an *in situ* sol–gel method. These binary TC NCs were then modified with chitosan at varying weight percentages (2%, 4%, 6%, and 8%). The resulting NCs were analyzed using various spectral tools. XRD analysis revealed the dominance of the anatase form of TiO_2 in both binary and ternary NCs. UV-visible DRS measurements were used to study the optical properties of the NCs and compare these to those of individual components. Microscopic analysis indicated the formation of grain clusters with irregular shapes, with particle sizes ranging between 10 and 20 nm. FT-IR analysis studied the interconnectivity between TC and chitosan through different functional moieties, while Raman analysis confirmed the phases of the different constituents. BET analysis showed that TCC 8 NCs (having 8% OF chitosan in TC NCs) had a surface area 1.4 times greater than bare TiO_2 NPs. Antibacterial and antifungal studies were conducted using standard protocols to test the prepared NCs against representative microbes. When coated on cowhide leather as microbicidal agents, the TCC 8 NCs-coated leather exhibited the highest microbicidal activity against *E. coli*, *S. aureus*, *B. cereus*, *P. vulgaris*, *C. albicans*, and *A. niger* in comparison to other ternary NCs, including TCC 2, TCC 4, and TCC 6, as well as binary NCs such as TC 10, TC 20, TC 30, and TC 50. This study showcases the effectiveness of these functional NCs for the surface disinfection of leather coatings.

Received 24th September 2024
Accepted 6th January 2025

DOI: 10.1039/d4ra06892k

rsc.li/rsc-advances

Introduction

TiO_2 nanomaterials are some of the promising candidates for antimicrobial studies due to ease of interaction with microbes, entering easily into the microbes, reactive oxygen species (ROS) under UV irradiation, *etc.* which lead to microbial inactivation. To enhance the microbial inactivation further, various strategies have been adopted for modifying the TiO_2 host materials. Among the different strategies, the composite formations of TiO_2 nanomaterials with other materials have tuned the physicochemical properties feasible for improving the overall antimicrobial efficiency. In this regard, nanostructured CuO has been utilized to modify the TiO_2, since CuO has auspicious antibacterial activity, anti-carcinogenic properties, low-cost, abundant nature, strong bactericidal properties as well as high stability. So, the composite of TiO_2 with CuO nanostructures exhibits encouraging outcomes in preventing the growth of microbes, showing a large surface area compared to bare TiO_2. So, such TiO_2–CuO nanocomposites (TC NCs) exhibit promising microbicidal activity.[1–3]

An enhancement in the photocatalytic inactivation performance of TiO_2 nanoparticles (NPs) can be understood to be due to the incorporation of CuO since it is responsible for enhancing defects within the TiO_2 lattice such as oxygen vacancies. Such vacancies also reduce the conduction band, thereby promoting activation of O^{2-} species.[4–6] In this connection, some endeavors have been illustrated earlier. Kubiak *et al.* reported the hydrothermally synthesized TC NCs, which reflected enhanced antimicrobial activity, but the NCs revealed diminished surface area compared to bare TiO_2.[7] In addition, surface modification of bare TiO_2 with CuO nanoclusters by radiolytic methods can decrease the photocatalytic activity under both visible as well as UV light, which affects microbicidal activity.[8,9] Along with the hydrothermal and radiolytic

[a]*Nanoscience Research Laboratory, Department of Chemistry, Shivaji University, Kolhapur 416 004, Maharashtra, India. E-mail: sdd_chem@unishivaji.ac.in*

[b]*Department of Chemistry, Yashwantrao Chavan Mahavidyalaya, Halkarni, Kolhapur, 416 552, Maharashtra, India*

[c]*School of Nanoscience and Biotechnology, Shivaji University, Kolhapur 416 004, Maharashtra, India*

[d]*Department of Microbiology, Shivaji University, Kolhapur 416 004, Maharashtra, India*

† Electronic supplementary information (ESI) available. See DOI: https://doi.org/10.1039/d4ra06892k

methods, other sophisticated synthesis methods have been deployed to design the aforementioned NCs. Banas-Gac *et al.* reported thin film bilayers of TC NCs deposited by RF reactive magnetron sputtering.[10] This technique can lead to the development of a bottom layer of CuO with a fixed thickness and a top layer of TiO_2 with a deliberately variable thickness. This is used to avoid spurious effects at the interface between layers to ensure efficient charge transfer.[10] Along with the aforementioned synthetic approaches, flame-assisted chemical vapour deposition (CVD) was deployed earlier for the same purpose.[11] This work demonstrated the effective use of TC NCs for antimicrobial study for food storage,[12,13] still there was a lag associated with instability of material at low temperatures. This can be further reflected by the slower production of ROS by said samples during the study.[14]

Though the representative studies regarding TC NCs have been conducted effectually, the prolonged scope can be achieved by seeking the use of an easy synthetic approach instead of sophisticated routes. A wet chemical approach such as the sol–gel method is one of the easiest synthetic approaches to designing NCs. So, the present investigation tends to utilize the same. In addition, as discussed above, though TC NCs exhibit good antibacterial properties, there is still a chance to enhance the biocompatibility, surface area, optoelectronic properties, energetic active sites at the surface, *etc.* And for this, carbon nanostructures, organic semiconductors, polymers, noble metal NPs, *etc.* have been effectually deployed.[15,16]

Particularly, chitosan (CS) has gained striking interest among existing polymers. This is due to its fascinating antibacterial activity, good biodegradation, outstanding biocompatibility, non-toxicity and excellent physicochemical properties.[17,18] In this manner, to alter the metal oxide's biological characteristics, CS biopolymer can be combined with metal oxides, due to its aforementioned characteristics.[19–21] In addition, the polymeric nature of CS can provide a strong bonding with the metal oxide surface, providing decent stability.[22,23] Hence, moving towards ternary TiO_2–CuO–chitosan (TCC) NCs can be an effective strategy, providing a novel opportunity to design and study said TiO_2-based NCs, as such microbicidal study for leather coating has not been done yet. This comprises the various aspects of microbicidal studies with promising microbicidal activity, biocompatibility, decent photocatalytic activity when exposed to UV light, chemical stability, non-toxicity, *etc.*

So, the present study focussed on the designing of ternary NCs for microbicidal study. This work includes the synthesis of binary TiO_2–CuO *i.e.* TC 10 NCs, TC 20 NCs, TC 30 NCs, and TC 50 NCs with varying content of CuO in 10, 20, 30, and 50 wt%, respectively. Also, the synthesis of ternary TiO_2–CuO–chitosan *i.e.* TCC 2 NCs, TCC 4 NCs, TCC 6 NCs, and TCC 8 NCs with varying content of CS in 2, 4, 6, and 8 wt%, respectively, by *in situ* sol–gel method and their characterizations using various sophisticated spectral/analytical tools. Thereafter, a good diffusion method was used to demonstrate the microbicidal study. For this, TC NCs and TCC NCs were exposed to fungal strains such as *Candida albicans* and *Aspergillus niger* as well as bacterial strains such as *E. coli*, *P. vulgaris*, *B. cereus*, and *S. aureus* under dark and light conditions.

Results and discussion

X-ray diffraction (XRD) pattern analysis

The structural properties of all samples were investigated by using XRD patterns as depicted in Fig. 1a. The XRD pattern of TiO_2 NPs was matched with the ICSD card number 75-1537,[24] reflecting the presence of the anatase phase. TiO_2 NPs exhibit the characteristic peaks at $2\theta = 25.140$, 37.930, 48.000, 54.060, and 55.040 that are attributed to the (101), (004), (200), (105), and (211) crystalline planes, respectively. Thereafter, these aforementioned peaks for NPs reveal their appropriate synthesis. In addition, the representative peaks at $2\theta = 32.57°$ (110), 35.62° (002), 38.75° (111), and 48.23° (202), within XRD patterns of TC 50 NCs, signify the existence of CuO NPs with TiO_2 lattice.[25] Thereafter, in the case of TCC 8 NCs, due to a slight amount of CS NPs, its preferred peak (at 20.16°) is not observed.[26] With an increase in the concentration of CS NPs in TC 50 NCs, the intensity of characteristic peaks of TC 50 NCs decreases, confirming the successful synthesis of ternary NCs.[27] This effect may result from the exfoliation and uniform anchoring of CS NPs onto TC 50 NCs.[28] The incorporation of CS

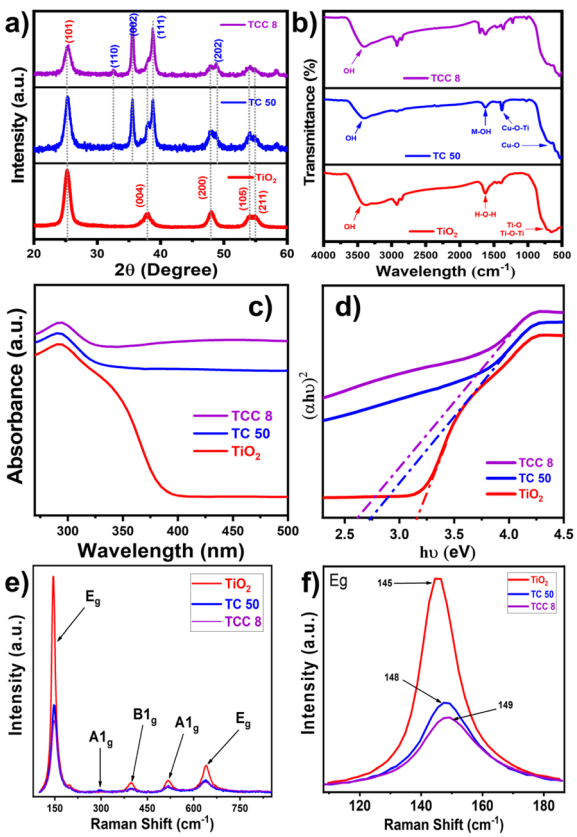

Fig. 1 (a) XRD patterns, (b) FT-IR spectra, (c) UV-visible DRS, (d) Tauc plots, (e) Raman spectra, and (f) localized magnified Raman spectra of bare TiO_2 NPs, TC 50 NCs with varying content of CuO (50 wt%), and TCC 8 NCs with varying content of CS NPs (8 wt%).

NPs and CuO NPs with TiO_2 NPs induces a distortion in the lattice structure, as evidenced by the broadening of the diffraction peak at 25.14° and the decrease in its intensity.[28] Such interactions may enhance the overall structural properties, as supported by crystallite size determination using the Debye–Scherrer equation. In addition, the XRD patterns of bare CuO NPs, CS NPs, binary TC NCs, as well as TCC NCs, are highlighted in Fig. S1, in ESI.† Also, the associated desired parameters of XRD analysis are described in Table S1, ESI.† Such distorted NCs can be effectual towards energetic surface areas with a high defective nature and higher active sites, useful for promoting antimicrobial assets.[29]

Fourier transform infrared (FT-IR) analysis

Fig. 1b shows FT-IR spectra of all samples, having a range of 4000–400 cm^{-1} at room temperature. For bare TiO_2 NPs, the broad bands observed in the range of 500–900 cm^{-1} are assigned to Ti–O and Ti–O–Ti bonds. A similar case is observed for bare CuO NPs, representing Cu–O bonds at a similar frequency range. As shown in Fig. 1b, the characteristic peak at 1383 cm^{-1} is assigned to stretching vibrations of Cu–O–Ti groups, confirming the successful incorporation of CuO with TiO_2 NPs.[30] In addition, these binary NCs possess the M–OH bond, represented by the peak at 1622 cm^{-1}, which provides the site for linking CS NPs to optimized NCs.[31,32] In addition, FT-IR spectra of ternary NCs along with that of CS NPs and optimized TC 10, TC 20, and TC 30 NCs are given in Fig. S2, ESI.† The characteristic peaks of CS NPs (around 1600–1200 cm^{-1}) can be easily seen in the TC 50 NCs. The intensity of these peaks is observed to be enhanced in TC 50 NCs, as the concentration of CS NPs is enhanced. This reveals the effective loading of CS NPs on said TC 50 NCs. In addition, for all samples, an intense broad band appeared in the 3200–3550 cm^{-1} region that was attributed to the –OH stretching vibration of surface hydroxyl groups of adsorbed water molecules. Hence, the associated functional moiety of synthesized NCs aligns well with that of bare TiO_2 NPs, which designates proper interconnectivity within samples.

UV-visible diffuse reflectance spectroscopy (UV-visible DRS) analysis

The UV-visible DRS spectra were used to investigate the optical characteristics of synthesized samples. Fig. 1c shows the UV-visible DRS spectrum of the bare TiO_2 NPs, TC 50, and TCC 8 NCs. This shows the redshift for TiO_2 NPs with the incorporation of CuO NPs with the lattice, revealing an improved optical property. This was further boosted with the loading of CS NPs on optimized TC 50 NCs. Such enhanced optical properties promoted the diminished band gap value of 2.61 eV from 2.74 eV (of TC 50 NCs) and 3.17 eV (of bare TiO_2 NPs), as shown in the inset Tauc plot (Fig. 1d). The UV-visible DRS spectra for other samples and their associated band gap values with band edges are shown in Fig. S3, ESI and mentioned in Table S2, ESI,† respectively. Hence, such composition of CuO NPs as well as CS NPs with TiO_2 NPs stimulate its absorption strength in the visible region, supporting to generation of the maximum ROS for inhibiting the bacterial zone in the presence of visible light irradiation.[18,33] When the material absorbs light of energy equal to or greater than its bandgap, electron–hole pairs (e^-/h^+) are generated. These e^-/h^+ pairs interact with molecular oxygen (O_2) and water (H_2O) to produce ROS, including superoxide anions ($O_2^{-\bullet}$), hydroxyl radicals ($^\bullet OH$), and hydrogen peroxide (H_2O_2). These ROS inflict oxidative damage on bacterial cell walls, proteins, and DNA, thereby enhancing antibacterial efficacy. The diminished bandgap and improved optical absorption in the visible region increase e^-/h^+ generation, maximizing ROS production and significantly improving the antibacterial performance of the composite under visible light irradiation.[34]

Raman analysis

Raman spectra of representative samples are shown in Fig. 1e. The samples exhibit characteristic peaks of the anatase TiO_2 phase in good agreement. The Eg peaks at 145 and 636 cm^{-1} correspond to the symmetric stretching vibration of O–Ti–O, and the B1g and A1g peaks at 394 and 514 cm^{-1} correspond to the symmetric and anti-symmetric bending vibrations of O–Ti–O, respectively. In addition, the characteristic peak at 291 cm^{-1} in spectra of TC 50 and TCC 8 NCs discloses due to CuO NPs.[25,35] An increase in the concentration of CuO NPs results in a lower intensity of the peaks, which is primarily due to the high dispersity of CuO NPs over the TiO_2 nanosheet's surface, sharing the surface O entities. Similarly, after loading CS NPs on optimized TC 50 NCs, there is a further reduction in the intensity of original peaks, signifying the integration of CS NPs to form ternary TCC NCs.[18] In addition, the Raman shift observed in the NCs compared to bare TiO_2 NPs, as shown in Fig. 1f, can be attributed to phase transitions and changes in bond strength, which arise from incorporating CuO and CS with the TiO_2 NPs.[36]

Microscopic analysis

The elemental composition analysis of the TCC 8 NCs was done using energy dispersive spectroscopy (EDS) analysis as shown in Fig. 2a. Herein, the characteristic peaks of the elemental Ti, Cu, C and O are observed, excluding any other peaks due to impurities. This can be claimed by seeing EDS spectra of bare TiO_2 NPs and TC 50 NCs as shown in Fig. S4, ESI.†[18] Hence, the respective EDS spectrum describes the existence of correct elemental compositions within desired NCs. In concern to the microscopic analysis of synthesized samples, scanning electron microscopy (SEM) images are shown in Fig. S5, ESI,† which discloses the desired morphology of the samples. Thereafter, Fig. 2b–d shows the transmission electron microscopy (TEM) image and selected area electron diffraction (SAED) pattern of TCC 8 NCs with different magnifications. TCC 8 NCs having highly aggregated NPs are of irregular shapes as compared to bare and binary NCs [Fig. S(6 and 7), ESI†]. This can contribute to the development of rougher surfaces with a highly porous structure, thereby enhancing the performance of the intended application.[37] These irregular shapes can be further understood by seeing SEM images as mentioned in Fig. S5, ESI.† Whereas, from TEM images [Fig. 2b and c], this can be revealed that the TiO_2, CuO as well as CS NPs are uniformly incorporated with each other.[38] Herein, the light grey and dark regions are of TiO_2

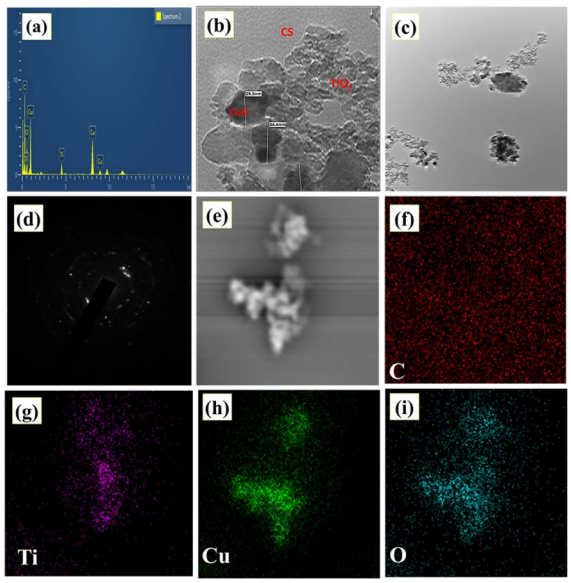

Fig. 2 (a) EDS spectrum, (b–d) TEM images, and (e–i) elemental mapping images of TCC 8 NCs representing elemental C, Ti, Cu, and O.

and CuO NPs, respectively (Fig. S7(a and b)†). In addition, the particle size of TCC 8 NCs was determined as 31 nm. The SAED pattern proved that TCC 8 NCs were polycrystalline in nature.[39] In addition, a uniform elemental distribution within TCC 8 NCs can be illustrated in Fig. 2e–i. Likewise, such elemental mapping dot images of bare TiO_2 and TC 50 NCs are shown in Fig. S(6 and 7), ESI.†

Brunauer–Emmett–Teller (BET) analysis

The N_2 adsorption–desorption isotherms of optimized samples are shown in Fig. 3a. These materials exhibit the type IV isotherms ascribed to the separation of N_2 adsorption and desorption curves. For said ternary as well as binary NCs, higher surface areas were observed as compared to bare TiO_2 NPs.[40] This may be due to the uniform distribution of NPs with each other, which can be supported by observing the aforementioned SEM and TEM images of the TC 50 NCs and TCC 8 NCs. In addition, the pore size of all samples in the range of 2.4 to 3.6 nm, confirms the mesoporous nature of all samples, which can be responsible for an improved microbicidal performance.[41] The said pore size was obtained through Fig. 3b, which shows the BJH (Barrett–Joyner–Halenda) curve, specific surface area and pore size from BET analysis are summarized in Table S3, ESI.† Hence, BET reveals the higher surface area for desired samples, which are associated with higher energetic surfaces as well as active sites with porous nature.[26] These observed surface properties may be significant for more access with the microbes, enhancing the microbicidal performance.[42]

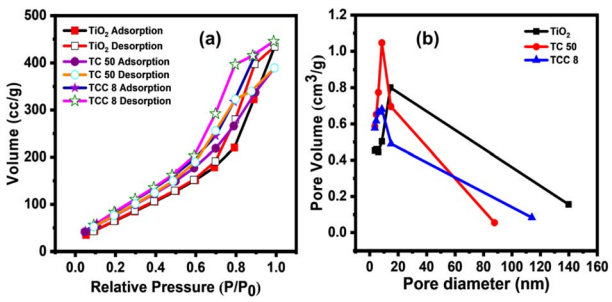

Fig. 3 (a) N_2 adsorption–desorption isotherms, and (b) BJH curves of bare TiO_2 NPs, TC 50 and TCC 8 NCs.

Setup for microbicidal study

Cytotoxicity study. The cytotoxicity of TC 50 and TCC 8 NCs was evaluated using an MTT assay on the L929 fibroblast cell line, with the culture medium being DMEM with high glucose (Cat No-11965-092) and FBS (Gibco, Invitrogen, Cat No-10270106), as shown in Fig. 4. Cells were initially incubated at a concentration of 1×10^4 cells per ml in the culture medium for 24 h at 37 °C with 5% CO_2. They were then seeded at a concentration of 1×10^4 cells per well in 100 μl of culture medium. Samples at concentrations of 2, 4, 6, 8, and 10 μg ml^{-1} were added to the microplates (tissue culture grade, 96 wells). Control wells contained 0.2% DMSO in PBS and a cell line. Each sample was tested in triplicate. Controls were used to determine the baseline cell survival and the percentage of live cells after incubation. Cell cultures were incubated for 24 h at 37 °C with 5% CO_2 in a CO_2 incubator. After incubation, the medium was completely removed, and 20 μl of MTT reagent (5 mg ml^{-1} in PBS) was added. Cells were then incubated for an additional 4 h at 37 °C in the CO_2 incubator, during which the formation of formazan crystals was observed under a microscope. Viable cells reduced the yellowish MTT to dark-colored formazan. After removing the medium, 200 μl of DMSO was added, and the samples were incubated for 10 minutes at 37 °C, protected from light by wrapping with aluminium foil. The absorbance of each sample was measured with a microplate reader at a wavelength of 550 nm.

Antibacterial study. *In vitro* microbicidal studies for binary TC NCs and ternary TCC NCs were assessed using the agar cup method. Initially, all samples, including binary and ternary NCs, were prepared in sterile distilled water (1000 μg ml^{-1}) to create stock solutions. From these stock solutions, 100 μl

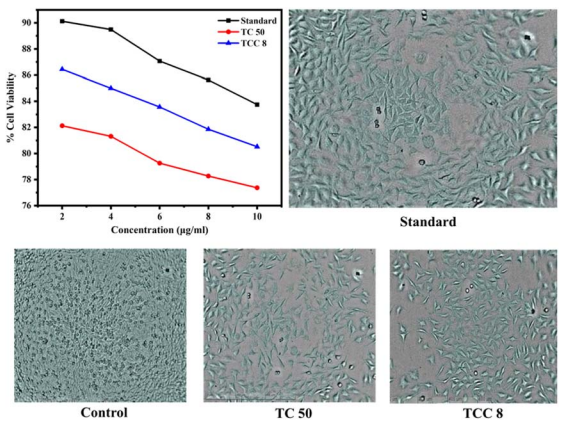

Fig. 4 Cytotoxic effect of standard (5-flurouracil), control, TC 50, and TCC 8 NCs on L929 fibroblast cell line.

samples were used to evaluate the antibacterial and antifungal activities of the binary and ternary NCs. DMSO was employed to dissolve the tested samples, and solutions with concentrations ranging from 10% to 50% were prepared in DMSO for the microbicidal study. The microbicidal activity of the NCs was evaluated using the agar cup method against Gram-positive species Bacillus cereus 2703 and *Staphylococcus aureus* NCIM 2654, and Gram-negative species *Escherichia coli* NCIM 2066 and *Proteus vulgaris* 2813. These bacterial strains, purchased from NCIM, NCL, Pune, India, were grown in nutrient broth to a log phase containing 10^8 CFU ml^{-1}. The bacterial cultures were then swabbed onto the surface of Mueller–Hinton agar plates.[43] Sterile culture media plates were prepared, and wells were created using a sterile cork borer (0.7 cm diameter). A 100 μl sample of the respective NCs concentrations was added to each well. The plates were allowed to diffuse in the refrigerator for 10 minutes before being incubated for 24 h at 37 °C. Streptomycin served as a positive control, and DMSO as a negative control, to compare the microbicidal activity of various NPs and NCs.[43,44]

Testing over leather. To prepare the NC solutions, dimethyl sulfoxide (DMSO) was used to dissolve the tested samples. Solutions with concentrations ranging from 10% to 50% were prepared in dimethyl sulfoxide (DMSO) to screen the microbicidal activity of bare TiO_2, CuO NPs, and TC 50 and TCC 8 NCs.

The agar cup method (well diffusion assay) was employed to assess the microbicidal activity of the synthesized NCs, as described previously.[45,46] The activity was tested against Gram-positive species *Bacillus cereus* 2703 and *Staphylococcus aureus* NCIM 2654, and Gram-negative species *Escherichia coli* NCIM 2066 and *Proteus vulgaris* 2813. These bacterial strains were purchased from NCIM, NCL, Pune, India. Log-phase bacterial cultures, containing 10^8 cfu ml^{-1} of each strain, were grown in Mueller–Hinton broth and then streaked aseptically onto sterile Mueller–Hinton agar plates.[45] Wells were created on the agar plates using a sterile cork borer (0.7 cm diameter), and 100 μl of the respective NPs and NCs solutions were added to each well. The plates were refrigerated for 10 minutes to allow diffusion and then incubated for 24 h at 37 °C, both in the presence and absence of light.[47] In this assay, Streptomycin was used as a positive control and dimethyl sulfoxide (DMSO) as a negative control to compare the microbicidal activity of the various NCs.[46,48]

For the antifungal activity, a similar procedure was followed. MGYP agar plates [Hi-Media] were prepared and inoculated with the fungal strain *Candida albicans* (NCIM 3466). The agar plates were incubated at 27 °C for 48 to 72 h. After incubation, the plates were examined for zones of inhibition around the wells. The microbicidal results were compared with a standard antifungal agent, Fluconazole (100 μg ml^{-1}), as a positive control and DMSO as a negative control.[49]

Cytotoxicity assay. The *in vitro* cell viability assay for TC 50 NCs and TCC 8 NCs was measured using an MTT reduction assay at Infinite Biotech, Institute of Research and Analysis, Sangli. L929 Fibroblast cell line was employed for cell viability assay. Fig. 4 showed lower cytotoxic activity of TC 50 NCs and TCC 8 NCs against L929 fibroblast cell lines compared to standard drug 5-Flurouracil,[50] which can also be perceived through Table 1. Based on this, TCC 8 NCs can demonstrate significantly lower cytotoxicity as compared to binary TC 50 NCs, emphasizing their potential as a safer and more effective alternative for leather coating applications.

Antibacterial activity. The microbicidal activity was measured based on the diameter of the zone of inhibition (Fig. 5) for binary TC NCs with varying content of CuO (10, 20, 30 & 50 wt%), and Fig. 6 for ternary TCC NCs with varying content of CS NPs (2, 4, 6 & 8 wt%).

Whereas, the results of the antibacterial assays are summarized in Tables 2–5 for binary TC 50 NCs, and ternary TCC 8 NCs, respectively. The zero activity observed for TC 20 and TC 30 against *S. aureus* is likely due to specific structural or physicochemical properties, such as limited surface area or poor dispersion stability, which may hinder their interaction with microbial cells. In contrast, TC 10 and TC 50 exhibit antimicrobial activity, likely due to optimal concentrations or superior

Table 1 Effects of the compound against L929 fibroblast cell line by MTT assay

Sr. no.	Sample code	Concentration (μg ml^{-1})	OD	Percentage of cell viability (%)	Percentage of inhibition (%)	IC50 (μg ml^{-1})
1	Control (lactic acid)	—	1.114	—	—	—
2	Standard (5-fluorouracil)	2	1.004	90.12	9.87	
		4	0.997	89.49	10.50	
		6	0.970	87.07	12.92	
		8	0.954	85.63	14.36	
		10	0.933	83.75	16.24	
3	TC 50	2	0.915	82.13	17.86	—
		4	0.906	81.32	18.67	
		6	0.883	79.26	20.73	
		8	0.872	78.27	21.23	
		10	0.862	77.37	22.62	
4	TCC 8	2	0.963	86.44	13.55	—
		4	0.947	85.00	14.99	
		6	0.931	83.57	16.42	
		8	0.912	81.86	18.13	
		10	0.897	80.52	19.47	

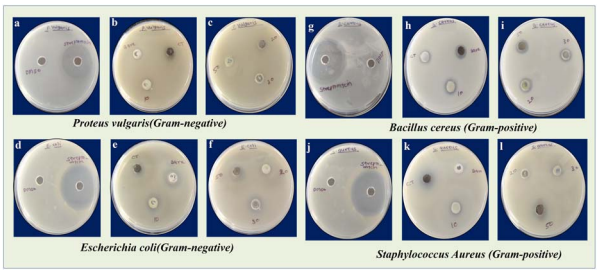

Fig. 5 Zone of inhibition observed for *P. vulgaris* (a–c), *E. coli* (d–f) and *B. cereus* (g–i), and *S. aureus* (j–l) of DMSO, Streptomycin, TiO_2, CuO, TC 10, TC 20, TC 30 and TC 50 NCs.

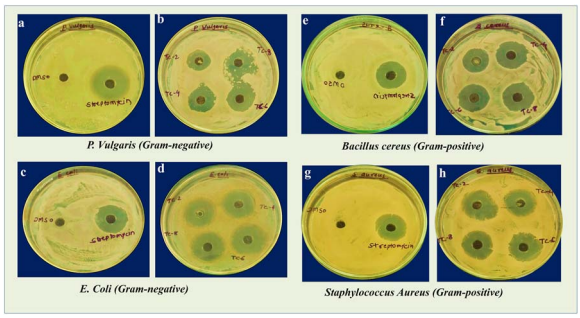

Fig. 6 Zone of inhibition observed for *P. vulgaris* (a and b), *E. coli* (c and d) and *B. cereus* (e and f), and *S. aureus* (g and h) of DMSO, Streptomycin, TCC 2, TCC 4, TCC 6, and TCC 8 NCs.

physicochemical characteristics that enhance their efficacy. All experiments were conducted in triplicates, ensuring the reproducibility of the results. The antibacterial activity of the optimized binary TC 50 NCs and ternary TCC 8 NCs showed that they exhibited excellent activity against Gram-positive and Gram-negative pathogens compared to other NCs.[51,52]

A detailed study was conducted to evaluate the actual microbicidal efficiency of coated leathers against fungi *C. albicans*, unicellular organisms. This study is presented in Fig. 7, showcasing the effectiveness of the optimized ternary TCC 8 NCs under various conditions, including dark and light environments. The results indicate a significant improvement in

Table 2 Zone of inhibition of TC 10, TC 20, TC 30, and TC 50 NCs against *S. aureus*, *B. cereus*, *E. coli*, and *P. vulgaris* in the presence of light and the absence of light

		Zone of inhibition of respective compounds in mm [in the presence of light]					
Sample	Test pathogens	BT	BC	TC 10	TC 20	TC 30	TC 50
Binary	*S. aureus*	11	18	15	00	00	15
	B. cereus	13	14	20	13	14	16
	E. coli	12	11	14	12	14	20
	P. vulgaris	18	13	00	10	12	14
		Zone of inhibition of respective compounds in mm [in the absence of light]					
Sample	Test pathogens	BT	BC	TC 10	TC 20	TC 30	TC 50
Ternary	*S. aureus*	08	10	11	00	00	13
	B. cereus	11	10	10	11	12	15
	E. coli	09	15	00	09	11	11
	P. vulgaris	12	10	00	12	14	12

Table 3 Positive and negative control associated with binary TC 50 NCs

	Zone of inhibition of positive and negative control in mm	
Test organism	Streptomycin	DMSO
Staph. aureus	35	00
B. cereus	32	00
E. coli	34	00
Proteus vulgaris	32	00

Table 4 Zone of inhibition of TCC 2, TCC 4, TCC 6 and TCC 8 NCs against *S. Aureus*, *B. cereus*, *E. coli* and *P. vulgaris* in the presence of light and the absence of light

		Zone of inhibition of respective compounds in mm [in the presence of light]			
Sample	Test pathogens	TCC 2	TCC 4	TCC 6	TCC 8
Binary	*S. aureus*	23	30	24	27
	B. cereus	20	21	25	26
	E. coli	21	30	31	27
	P. vulgaris	19	20	21	23
		Zone of inhibition of respective compounds in mm [in the absence of light]			
Sample	Test pathogens	TCC 2	TCC 4	TCC 6	TCC 8
Ternary	*S. aureus*	20	26	21	24
	B. cereus	16	17	21	22
	E. coli	20	24	22	19
	P. vulgaris	21	19	20	21

Table 5 Positive and negative control associated with ternary TCC 8 NCs

	Zone of inhibition of positive and negative control in mm	
Test organism	Streptomycin	DMSO
S. aureus	26	00
B. cereus	26	00
E. coli	35	00
P. vulgaris	25	00

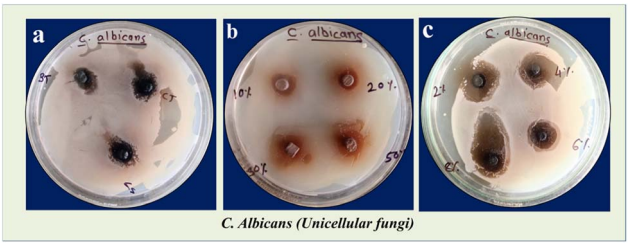

Fig. 7 Microbicidal activity showing zone of inhibition for (a) bare TiO_2 NPs *i.e.* BT, bare CuO NPs *i.e.* CT and bare chitosan *i.e.* CS, (b) TC 10, TC 20, TC 30, and TC 50 NCs, and (c) TCC 2, TCC 4, TCC 6, and TCC 8 NCs against *C. albicans*.

microbicidal efficiency when compared to bare TiO_2, CuO NPs, and optimized binary TC 50 NCs.

The outcomes of the microbicidal assays on coated leathers are consolidated in Table 6, delineating the efficacy of bare TiO_2, CuO NPs, binary TC 10, TC 20, TC 30, and TC 50 NCs, as well as ternary TCC 2, TCC 4, TCC 6, and TCC 8 NCs, respectively, against the fungal species *C. albicans*, which are unicellular organisms. The enhanced microbicidal efficiency of TCC 8 NCs can be attributed to several factors. Firstly, these NCs possess a higher surface area, allowing for increased interaction with microorganisms. Additionally, their porous nature facilitates better penetration and contact with fungal cells, leading to improved microbicidal activity. Importantly, TCC 8 NCs exhibit lower cytotoxicity compared to bare TiO_2, CuO NPs, and TC 50 NCs, making them a safer and more effective option for leather coatings.

Table 6 Zone of inhibition of binary bare TiO_2, CuO NPs, TC 10, TC 20, TC 30, TC 50 NCs as well as ternary TCC 2, TCC 4, TCC 6, TCC 8 NCs against *C. albicans* in the presence of light and the absence of light

		Zone of inhibition of respective compounds in mm [in the presence of light]					
Sample	Test pathogens	BT	BC	TC 10	TC 20	TC 30	TC 50
1	*Candida albicans*	10	10	15	14	11	12
		Zone of inhibition of respective compounds in mm [in the absence of light]					
Sample	Test pathogens	BT	BC	TC 10	TC 20	TC 30	TC 50
1	*Candida albicans*	08	10	11	00	00	11

		Zone of inhibition of respective compounds in mm [in the presence of light]			
Sample	Test pathogens	TCC 2	TCC 4	TCC 6	TCC 8
1	*Candida albicans*	11	11	19	14
		Zone of inhibition of respective compounds in mm [in the absence of light]			
Sample	Test pathogens	TCC 2	TCC 4	TCC 6	TCC 8
1	*Candida albicans*	00	05	11	12

Minimum inhibitory concentration. The study demonstrated that NCs exhibit good antimicrobial activity against the tested pathogens, with *B. cereus* showing notable sensitivity. Therefore, *B. cereus* was selected for further minimum inhibitory concentration (MIC) studies of the NCs. For the MIC study, different concentrations of NCs (10, 25, 50, 75, and 100 μg mL^{-1}) were prepared in DMSO. The MIC was determined to identify the lowest concentration of NCs that inhibits the growth of the test organisms. Suspensions of the test organism were prepared in sterile saline and spread onto Mueller–Hinton agar. Wells were created on the plates using a sterile cork borer.[55] Different concentrations (10, 25, 50, 75, and 100 μg mL^{-1}) of 100 μl NCs solutions were added to the wells. The plates were then incubated at 37 °C for 24 h to assess the

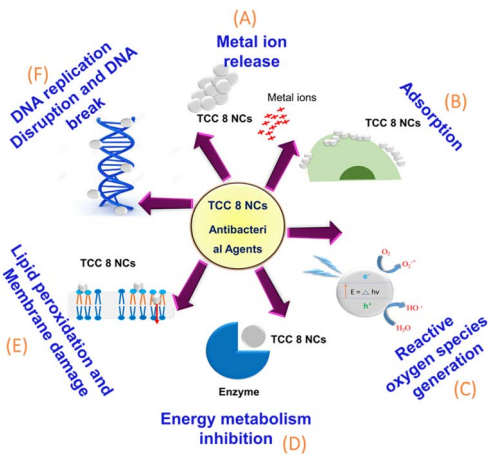

Fig. 8 Schematic representation of the antimicrobial mechanism of TCC 8 NCs illustrating the sequential steps (A to D) upon interaction with microbial cells.

The antimicrobial mechanism of TCC 8 NCs involves multiple interconnected processes, including surface contact with microbial cells, destruction of intracellular biomolecules, inhibition of protein and nucleic acid synthesis, disruption of metabolic functions, cellular disintegration, and the production of ROS under photon exposure. The enhanced antimicrobial efficacy of TCC 8 NCs is primarily attributed to their photocatalytic generation of ROS, such as $^{\bullet}OH$, $O_2^{-\bullet}$, and H_2O_2. These ROS inflict oxidative damage on vital cellular components, including lipids, proteins, and nucleic acids. Additionally, TCC 8 NCs release ions that penetrate bacterial cell walls, causing structural damage, membrane disruption, and further compromising the integrity of bacterial cells.[53,54] The primary factors driving the antimicrobial activity of TCC 8 NCs include their interaction with microbial cells, ion release, penetration resulting in cell wall damage and functional disruption, ROS generation under photo-irradiation, and subsequent DNA damage, as depicted in Fig. 8.

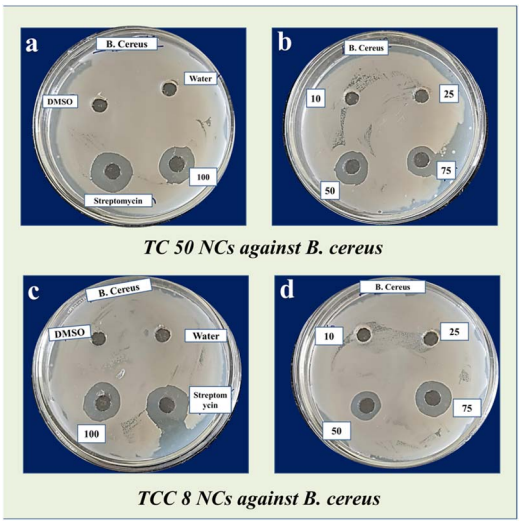

Fig. 9 MIC of B. Cereus showing zone of inhibition for (a and b) TC 50 NCs at different concentrations (10, 25, 50, 75, and 100 μg mL^{-1}), (c and d) TCC 8 NCs at different concentrations (10, 25, 50, 75, and 100 μg mL^{-1}).

inhibitory effect of the NPs on B. cereus. The zone of inhibition is shown in Fig. 9 and results are recorded in Table 7.

From this study, we conclude that the MIC for TC 50 and TCC 8 NCs is 50 μg ml^{-1}, as antimicrobial activity was observed at this concentration. Additionally, it was noted that the antimicrobial activity increased as the concentration of NCs increased beyond 50 μg ml^{-1}. The MTT assay indicated that the NCs exhibited biocompatibility and low cytotoxicity. In this study, TCC 8 NCs were found to be more effective than TC 50 NCs against clinical strains of *B. cereus*. A concentration of 50 μg ml^{-1} of both NCs demonstrated antibacterial activity without cytotoxicity to human cells, suggesting their potential use as antibacterial agents.[55,56]

Table 7 Zone of inhibition of binary TC 50 NCs as well as ternary TCC 8 NCs against *B. cereus* in the presence of light and the absence of light

TC 50 in presence of light					
Test pathogen	Zone of inhibition in mm				
Concentration	10 μg ml^{-1}	25 μg ml^{-1}	50 μg ml^{-1}	75 μg ml^{-1}	100 μg ml^{-1}
B. cereus	00	00	21	23	27
TCC 8 in presence of light					
B. cereus	00	00	23	25	27

Positive and negative control			
	Zone of inhibition in mm		
Test pathogen	DMSO	Water	Streptomycin
B. cereus	00	00	29

Traditionally, antimicrobial compounds or antibiotic potential were measured in the form of the zone of inhibition *i.e.* millimeter or centimetre.[57] MICs are defined as the lowest concentration of an antimicrobial that will inhibit the visible growth of a microorganism after overnight incubation.[58] In the current study, MIC of particular NCs was done by agar well diffusion method, at 50 μg ml^{-1} concentration both TC 50 and TCC 8 NCs show the zone of inhibition, here higher potency was considered based on higher zone of inhibition.

Some research paper suggests that as the concentration of NCs increases zone of inhibition increases but at certain concentrations NCs show a saturation effect and show the same or no zone of inhiation.[59] Hence at 100 μg ml^{-1} contraction TC 50 and TCC 8 NCs show same zone of inhibition.

Experimental section

Materials

All chemicals used were of analytical grade and used as received without further purification. Bare TiO_2 NPs were synthesized by the sol–gel method as reported earlier by our group.[60] While, for CuO NPs synthesis, the same method was deployed but with petite modification. The aforementioned synthesizes are described in ESI.†

Synthesis of TiO_2–CuO NCs

TC NCs were prepared using an *in situ* sol–gel route with a different composition of the content of CuO NPs (such as 10, 20, 30, and 50 wt%). Synthesized CuO NPs were added immediately after the complete precipitation of titanium hydroxide $[Ti(OH)_4]$ within the running route of TiO_2 NP synthesis. The final blackish-colored precipitates were formed, which were followed by washing, drying, and annealing as discussed in ESI.† The synthesized samples were assigned as TC 10, TC 20, TC 30, and TC 50 NCs having CuO NP content of 10, 20, 30, and 50 wt%, respectively.

Synthesis of TiO_2–CuO–chitosan NCs

An *in situ* sol–gel method was used for synthesizing TCC NCs with varying content of commercial CS NPs (such as 2, 4, 6, and 8 wt%). The CS NPs were dispersed in distilled water (DW) using a probe sonicator. These chitosan solutions were added directly during the synthesis of the TC NCs route after the hydroxylation of TC precursors. The blackish-colored precipitates were formed, which were subsequently washed, dried, and annealed at 450 °C for 2 h. Then these samples were designated as TCC 2, TCC 4, TCC 6, and TCC 8 NCs for 2, 4, 6, and 8 wt% of CS NPs, respectively, within binary NCs.

Preparation of nanoparticles finished leather discs and its microbicidal activity

Leathers were cut into circular pieces (8 mm diameter × 1.0 mm thick).[61] A cleaning treatment was performed to remove all impurities. Different concentrations of NCs were prepared in dimethyl sulfoxide (DMSO), and 100 μl of the NCs solution was infused onto the surface of each leather disc using

a micropipette.[62] The discs were then dried at room temperature and prepared for further antifungal activity testing. Before testing, the NP-infused leather discs were subjected to UV treatment for 10 minutes to sterilize the surfaces and prevent contamination during the experiments. For the antifungal activity tests, sterile Muller–Hinton agar plates were used. The respective test organisms were spread on the sterile plates, and the leather discs were placed aseptically on the surface. The plates were incubated at 37 °C for 24 h.

Characterization tools

The Bruker, AXS D8 Advance was used to obtain the powder XRD patterns of the samples. FT-IR spectra were obtained using an FT-IR spectrometer (Bruker, Germany ALPHA). Optical properties were studied using UV-visible DRS through a UV-visible spectrophotometer (LABINDIA, UV 3092). Raman spectra were obtained using a Raman spectrometer (Bruker MultiRAM, Germany). Microscopic analysis was done using TEM + EDS (JEM-2100F JEOL, Japan) operating at 125 kV. SEM images were analyzed using (JEOL Ltd Japan, JSM-6360). Surface area and pore size analysis were carried out using a BET surface analyzer (Quantachrome NOVA1000e, USA).

Conclusions

The microbicidal activity of the NCs is significantly improved by the composite of TiO_2 and CuO NPs with CS NPs. The NCs demonstrate long-lasting protection against the growth of microbes on leather surfaces through their robust coating performance as compared to bare TiO_2 NPs. This durability is crucial for applications in sectors like leather production of leather goods, where microbial contamination can lead to product deterioration. TCC NCs were prepared using an *in situ* sol–gel route with a different composition of the content of CS NPs (such as 2, 4, 6, and 8 wt%) for microbicidal application. The instrumental and spectroscopic techniques have revealed its chemical and structural properties. At the different concentrations of samples, TC 50 NCs and TCC 8 NCs showed a low percent inhibition against the L929 fibroblast cell line compared to standard drug 5-Fluorouracil. In the microbicidal assay, experimentally obtained results showed that the said TCC 8 NCs show excellent microbicidal activities with respect to other ternary NCs, including TCC 2, TCC 4, and TCC 6, as well as binary NCs such as TC 10, TC 20, TC 30, and TC 50; this can be used in leather coating. In addition, TCC 8 NCs showed the good antibacterial as well as antifungal activity in the presence of light as compared to in the absence of light. The functional TCC 8 NCs offer improved microbicidal activity, biocompatibility, and the potential for multifunctionality, making them a promising option for creating sophisticated microbicidal coatings for leather objects. With these regards, TCC 8 NCs have prospects for the development of multi-functional coatings in addition to their microbicidal qualities. For example, they can enhance the value of leather objects in a variety of applications by offering UV protection, water repellency, and even self-cleaning capabilities. Further investigation and advancement in this field may yield inventive approaches to enhancing leather goods' lifespan, hygienic qualities, and sustainability.

Data availability

The data supporting this article have been included as part of the ESI.†

Author contributions

Experimental work was designed by V. S. G. All synthesis parts have been completed by V. S. G. Antimicrobicidal study, cytotoxic assay, and coatings on leather were done by V. S. G., S. D. D., V. B. M., and K. D. S. Thereafter, V. S. G. and P. A. K. analyzed whole data and wrote the entire manuscript. Then, S. D. D. and other co-authors reviewed the manuscript.

Conflicts of interest

There are no conflicts to declare.

References

1 H. M. Yadav, S. V. Otari, R. A. Bohara, S. S. Mali, S. H. Pawar and S. D. Delekar, *J. Photochem. Photobiol., A*, 2014, **294**, 130–136.
2 S. P. Deshmukh, S. B. Mullani, V. B. Koli, S. M. Patil, P. J. Kasabe, P. B. Dandge, S. A. Pawar and S. D. Delekar, *Photochem. Photobiol.*, 2018, **94**, 1249–1262.
3 A. M. Alotaibi, B. A. D. Williamson, S. Sathasivam, A. Kafizas, M. Alqahtani, C. Sotelo-Vazquez, J. Buckeridge, J. Wu, S. P. Nair, D. O. Scanlon and I. P. Parkin, *ACS Appl. Mater. Interfaces*, 2020, **12**, 15348–15361.
4 C. Pan, H. Shen, G. Liu, X. Zhang, X. Liu, H. Liu, P. Xu, W. Chen, Y. Tian, H. Deng, H. Sun, J. Wang, Z. Luo, L. Zhang and Y. Guo, *ACS Appl. Nano Mater.*, 2022, **5**, 10980–10990.
5 M. Azizi-Lalabadi, A. Ehsani, B. Divband and M. Alizadeh-Sani, *Sci. Rep.*, 2019, **9**, 1–10.
6 A. M. Khalil, S. M. El-Sayed and A. M. Youssef, *Biomass Convers. Biorefin.*, 2023, 1–10.
7 A. Kubiak, K. Siwińska-Ciesielczyk, J. Goscianska, A. Dobrowolska, E. Gabała, K. Czaczyk and T. Jesionowski, *Mater. Sci. Eng., C*, 2019, **104**, 109839.
8 M. G. Méndez-Medrano, E. Kowalska, A. Lehoux, A. Herissan, B. Ohtani, D. Bahena, V. Briois, C. Colbeau-Justin, J. L. Rodríguez-López and H. Remita, *J. Phys. Chem. C*, 2016, **120**, 5143–5154.
9 A. Ślosarczyk, I. Klapiszewska, A. Parus, S. Balicki, K. Kornaus, B. Gapiński, M. Wieczorowski, K. A. Wilk, T. Jesionowski and Ł. Klapiszewski, *Sci. Rep.*, 2023, **13**, 1–16.
10 J. Banas-Gac, M. Radecka, A. Czapla, E. Kusior and K. Zakrzewska, *Appl. Surf. Sci.*, 2023, **616**, 156394.
11 H. A. Foster, D. W. Sheel, P. Evans, P. Sheel, S. Varghese, S. O. Elfakhri, J. L. Hodgkinson and H. M. Yates, *Chem. Vap. Depos.*, 2012, **18**, 140–146.

12 S. Zhang, X. Gong, Q. Shi, G. Ping, H. Xu, A. Waleed and G. Li, *ACS Omega*, 2020, **5**, 15942–15948.
13 V. K. Yemmireddy, G. D. Farrell and Y. C. Hung, *J. Food Sci.*, 2015, **80**, N1903–N1911.
14 P. Kumari, P. K. Panda, E. Jha, K. Kumari, K. Nisha, M. A. Mallick and S. K. Verma, *Sci. Rep.*, 2017, **7**, 1–17.
15 A. Guarnieri, M. Triunfo, C. Scieuzo, D. Ianniciello, E. Tafi, T. Hahn, S. Zibek, R. Salvia, A. De Bonis and P. Falabella, *Sci. Rep.*, 2022, **12**, 1–12.
16 E. I. Rabea, M. E.-T. Badawy, C. V. Stevens, G. Smagghe and W. Steurbaut, *Biomacromolecules*, 2003, **4**, 1457–1465.
17 R. C. Goy, S. T. B. Morais and O. B. G. Assis, *Rev. Bras. Farmacogn.*, 2016, **26**, 122–127.
18 M. Ikram, A. Shahzadi, S. Hayat, W. Nabgan, A. Ul-Hamid, A. Haider, M. Noor, S. Goumri-Said, M. B. Kanoun and S. Ali, *RSC Adv.*, 2022, **12**, 16991–17004.
19 S. C. Moratti and J. D. Cabral, *Antibacterial Properties of Chitosan*, Woodhead Publishing, 2017, vol. 1, pp. 31–44.
20 N. E. A. El-Naggar, A. M. Shiha, H. Mahrous and A. B. A. Mohammed, *Sci. Rep.*, 2022, **12**, 1–19.
21 M. Kucharska, M. Sikora, K. Brzoza-Malczewska and M. Owczarek, *Chitin Chitosan Prop. Appl.*, John Wiley & Sons, Ltd, 2019, pp. 169–187.
22 M. A. Mohammad, F. Y. Faris Taufeq, S. Suleman Ismail Abdalla and H. Katas, *RSC Adv.*, 2022, **12**, 19297–19312.
23 G. D. Jovanović, A. S. Klaus and M. P. Nikšić, *Rev. Argent. Microbiol.*, 2016, **48**, 128–136.
24 T. M. H. Nguyen and C. W. Bark, *ACS Omega*, 2020, **5**, 2280–2286.
25 H. Hamad, M. M. Elsenety, W. Sadik, A. G. El-Demerdash, A. Nashed, A. Mostafa and S. Elyamny, *Sci. Rep.*, 2022, **12**, 1–20.
26 P. S. Pawar, P. A. Koyale, V. S. Ghodake, S. V Mulik, Y. G. Kapdi, S. S. Soni, N. B. Mullani and S. D. Deleakr, *New J. Chem.*, 2023, **47**, 21825–21833.
27 B. Abarna, T. Preethi and G. R. Rajarajeswari, *J. Mater. Sci. Mater. Electron.*, 2019, **30**, 21355–21368.
28 M. M. Hasan and N. K. Allam, *RSC Adv.*, 2018, **8**, 37219–37228.
29 V. H. Rathi, A. R. Jeice and K. Jayakumar, *Appl. Surf. Sci. Adv.*, 2023, **18**, 1–13.
30 A. Kubiak, Z. Bielan, M. Kubacka, E. Gabała, A. Zgoła-Grześkowiak, M. Janczarek, M. Zalas, A. Zielińska-Jurek, K. Siwińska-Ciesielczyk and T. Jesionowski, *Appl. Surf. Sci.*, 2020, **520**, 146344.
31 L. S. Chougala, M. S. Yatnatti, R. K. Linganagoudar, R. R. Kamble and J. S. Kadadevarmath, *J. Nano- Electron. Phys.*, 2017, **9**, 04005.
32 R. Abazari, A. R. Mahjoub and S. Sanati, *RSC Adv.*, 2014, **4**, 56406–56414.
33 S. D. Delekar, A. G. Dhodamani, K. V. More, T. D. Dongale, R. K. Kamat, S. F. A. Acquah, N. S. Dalal and D. K. Panda, *ACS Omega*, 2018, **3**, 2743–2756.
34 Y. Li, W. Zhang, J. Niu and Y. Chen, *ACS Nano*, 2012, **6**, 5164–5173.
35 L. Li, X. Chen, X. Quan, F. Qiu and X. Zhang, *ACS Omega*, 2023, **8**, 2723–2732.
36 M. K. Date, L. H. Yang, T. Y. Yang, K. ye Wang, T. Y. Su, D. C. Wu and Y. L. Cheuh, *Nanoscale Res. Lett.*, 2020, **15**, 1–12.
37 S. Jayanthi, N. Krishnarao Eswar, S. A. Singh, K. Chatterjee, G. Madras and A. K. Sood, *RSC Adv.*, 2016, **6**, 1231–1242.
38 M. Behera, F. Othman Alqahtani, S. Chakrabortty, J. Nayak, S. Banerjee, R. Kumar, B.-H. Jeon and S. K. Tripathy, *ACS Omega*, 2023, **8**, 42164–42176.
39 M. Behera, F. O. Alqahtani, S. Chakrabortty, J. Nayak, S. Banerjee, R. Kumar, B.-H. Jeon and S. K. Tripathy, *ACS Omega*, 2023, **8**, 42164–42176.
40 M. Behera, F. O. Alqahtani, S. Chakrabortty, J. Nayak, S. Banerjee, R. Kumar, B. Jeon and S. K. Tripathy, *ACS Omega*, 2023, **8**, 42164–42176.
41 I. Mondal and U. Pal, *Phys. Chem. Chem. Phys.*, 2016, **18**, 4780–4788.
42 L. Yu, Y. Zhang, B. Zhang and J. Liu, *Sci. Rep.*, 2014, **4**, 1–5.
43 S. R. Waghmare, M. N. Mulla, S. R. Marathe and K. D. Sonawane, *3 Biotech*, 2015, **5**, 33–38.
44 M. A. Ibrahim, G. M. Nasr, R. M. Ahmed and N. A. Kelany, *Sci. Rep.*, 2024, 1–16.
45 S. V. Otari, R. M. Patil, N. H. Nadaf, S. J. Ghosh and S. H. Pawar, *Environ. Sci. Pollut. Res.*, 2014, **21**, 1503–1513.
46 R. Gurav, S. K. Surve, S. Babar, P. Choudhari, D. Patil, V. More, S. Sankpal and S. Hangirgekar, *Org. Biomol. Chem.*, 2020, **18**, 4575–4582.
47 M. Khan, M. Rafi Shaik, S. Tabrez Khan, S. Farooq Adil, M. Kuniyil, M. Khan, A. A. Al-Warthan, M. R. H. Siddiqui and M. Nawaz Tahir, *ACS Omega*, 2020, **5**, 1987–1996.
48 V. Kumaravel, K. M. Nair, S. Mathew, J. Bartlett, J. E. Kennedy, H. G. Manning, B. J. Whelan, N. S. Leyland and S. C. Pillai, *Chem. Eng. J.*, 2021, **416**, 129071.
49 P. Ubale, S. Mokale, S. More, S. Waghamare, V. More, N. Munirathinam, S. Dilipkumar, R. K. Das, S. Reja, V. B. Helavi and S. P. Kollur, *J. Mol. Struct.*, 2022, **1251**, 131984.
50 F. Hajareh Haghighi, M. Mercurio, S. Cerra, T. A. Salamone, R. Bianymotlagh, C. Palocci, V. Romano Spica and I. Fratoddi, *J. Mater. Chem. B*, 2023, **11**, 2334–2366.
51 K. S. Khashan, G. M. Sulaiman and F. A. Abdulameer, *Arabian J. Sci. Eng.*, 2016, **41**, 301–310.
52 N. R. Dhineshbabu and V. Rajendran, *IET Nanobiotechnol.*, 2016, **10**, 13–19.
53 V. Rodríguez-González, S. Obregón, O. A. Patrón-Soberano, C. Terashima and A. Fujishima, *Appl. Catal., B*, 2020, **270**, 118853.
54 S. Chen, Y. Guo, H. Zhong, S. Chen, J. Li, Z. Ge and J. Tang, *Chem. Eng. J.*, 2014, **256**, 238–246.
55 J. A. Shaik and R. K. Reddy, *Contemp. Clin. Dent.*, 2017, **8**, 11–19.
56 F. Kakian, E. Mirzaei, A. Moattari, S. Takallu and A. Bazargani, *BMC Res. Notes*, 2024, **17**, 1–6.
57 J. Hudzicki, *Am. Soc. Microbiol.*, 2012, 1–13.
58 A. Murugappan, J. S. Sudarsan and A. Manoharan, *J. Ind. Pollut. Control*, 2006, **22**, 149–160.

59 C. López de Dicastillo, M. Guerrero Correa, F. B. Martínez, C. Streitt and M. José Galotto, *Antimicrob. Resist. – A One Heal. Perspect.*, 2021, pp. 1–18.
60 V. B. Koli, A. G. Dhodamani, A. V. Raut, N. D. Thorat, S. H. Pawar and S. D. Delekar, *J. Photochem. Photobiol., A*, 2016, **328**, 50–58.
61 I. Carvalho, S. Ferdov, C. Mansilla, S. M. Marques, M. A. Cerqueira, L. M. Pastrana, M. Henriques, C. Gaidau, P. Ferreira and S. Carvalho, *Sci. Technol. Mater.*, 2018, **30**, 60–68.
62 V. J. Boyle, M. E. Fancher and R. W. Ross, *Antimicrob. Agents Chemother.*, 1973, **3**, 418–424.